a)

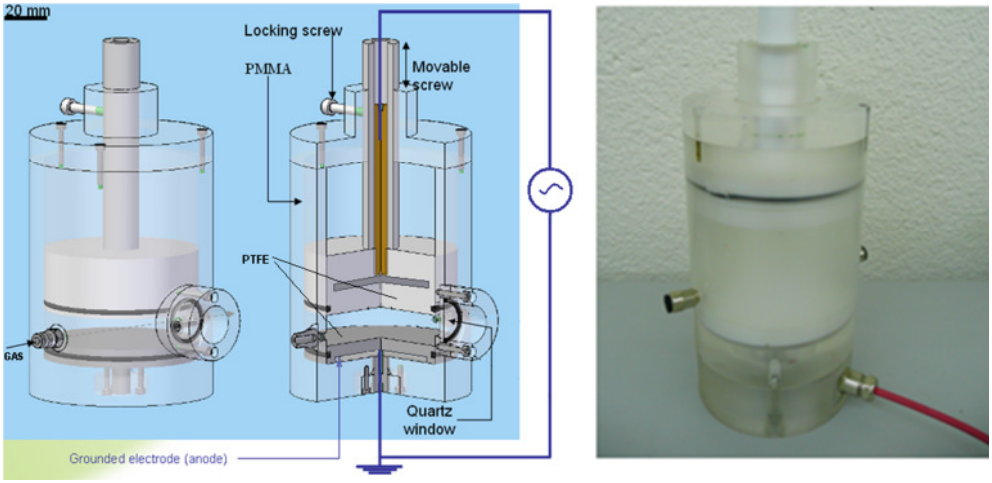

b)

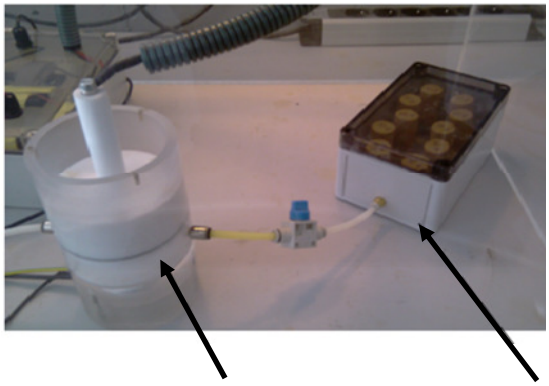

c)

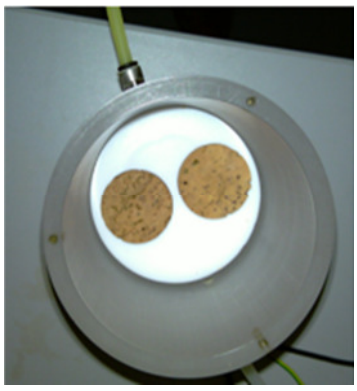

Figure 1: a) Schematic and photo of the in the NEATCORK project investigated DBD plasma sources. b) Experimental set-up for the remote treatment of cork stoppers enclosed in container where active species generated by the DBD are fed through. c) Experimental set-up for the treatment of cork disks integrated in the dielectrical material for a direct treatment of the cork material.

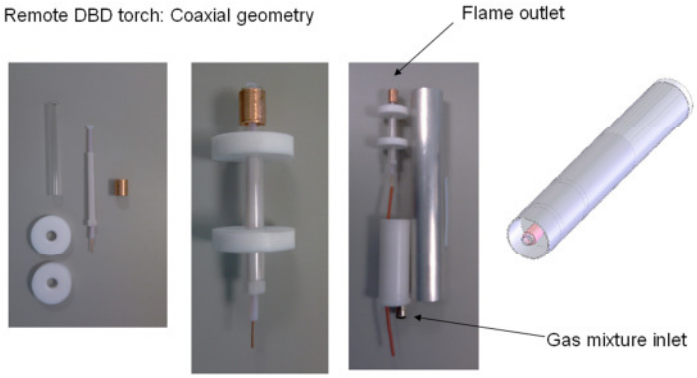

Figure 2: Photos of the DBD plasma jet developed during the NEATCORK project.

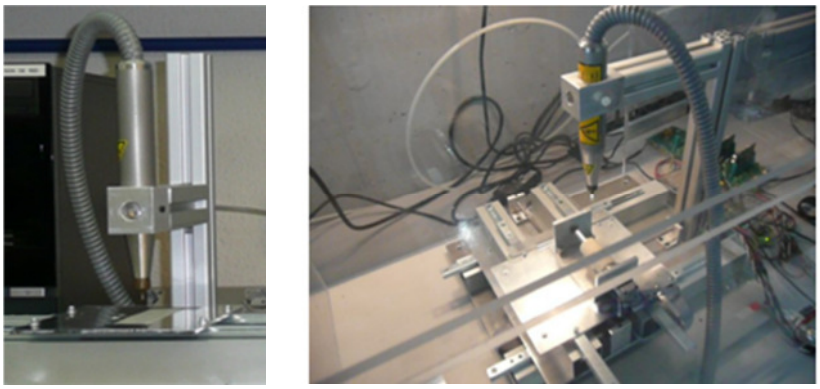

Figure 3: Photo of the in the NEATCORK investigated corona-based plasma torch (left side) and the experimental set-up for the treatment of cork stoppers with the corona-based plasma torch (right side).

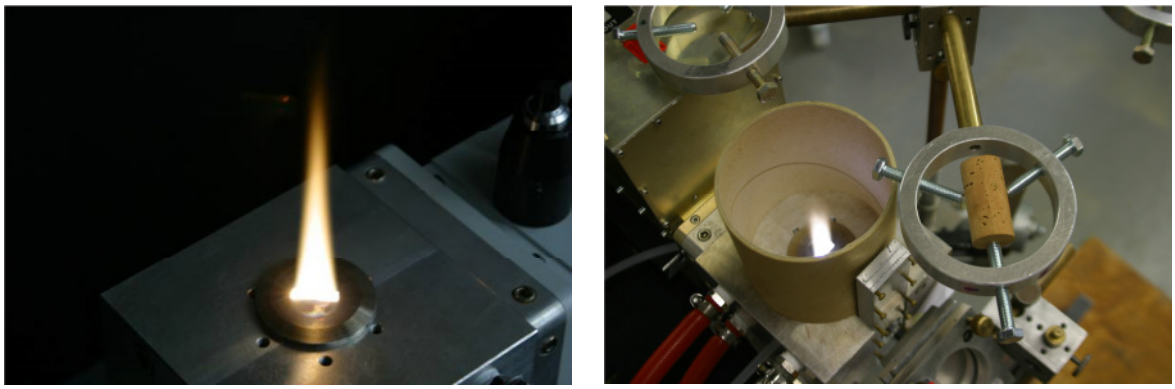

Figure 4: Photo of the in the NEATCORK investigated microwave plasma torch (left side) and the experimental set-up for the treatment of cork stoppers with the microwave plasma torch (right side).

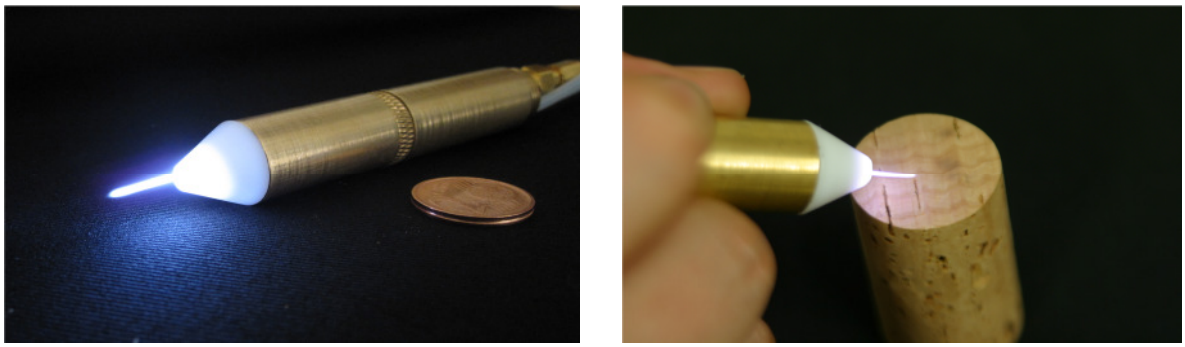

Figure 5: Photo of the in the NEATCORK investigated microwave micro plasma jet (left side) and the principle how the cork stoppers were treated with the microwave micro plasma jet: The treatment was conducted line by line by hand (right side).

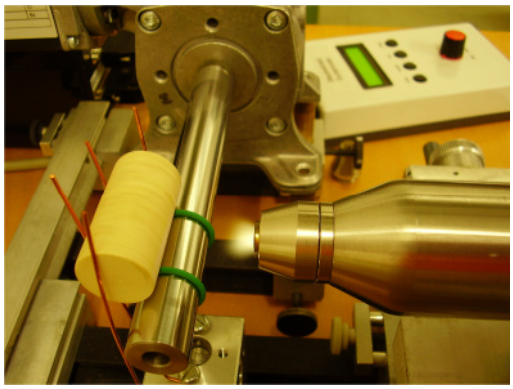

Figure 6: Photo of the experimental set-up for the treatment of cork stoppers with the corona-based plasma jet.

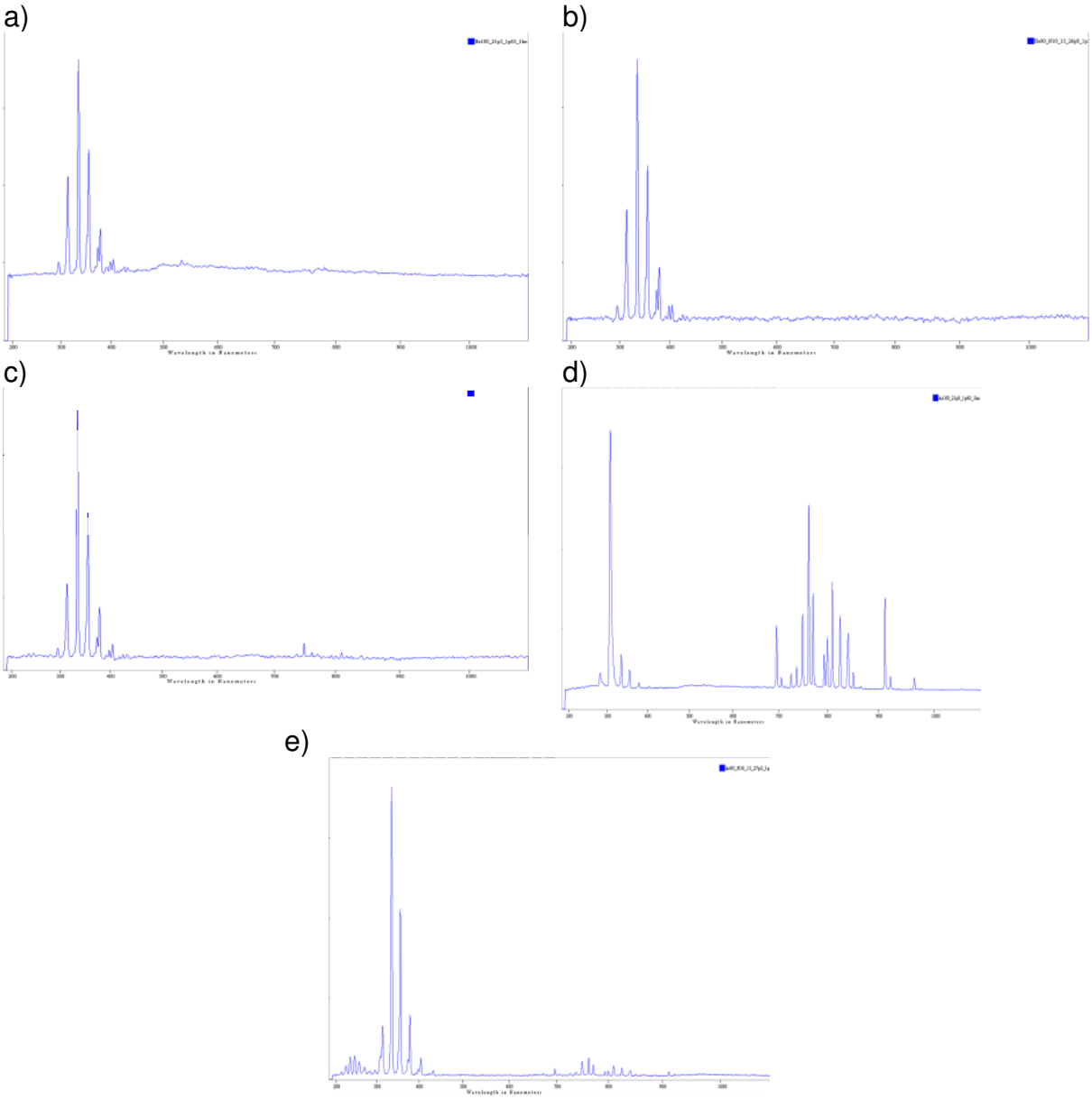

Figure 7: Spectroscopic investigations of the DBD plasma. Overview spectra of the DBD plasma for different gas mixtures. a) 100% helium, b) He-N_2-mixture (10-90%), c) He-Ar-N_2-mixture (40-40-20%), d) 100% argon and Ar-N_2-mixture (10-90%).

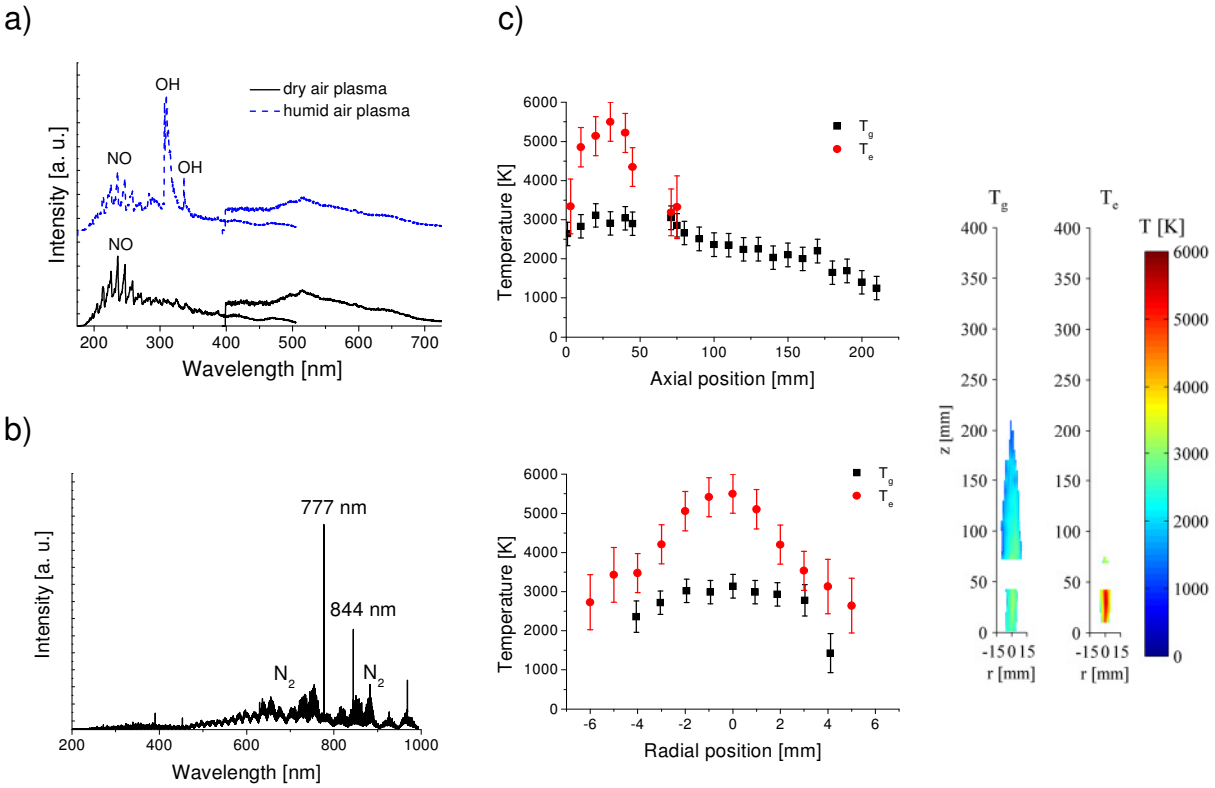

Figure 8: Spectroscopic characterisation of the microwave generated plasma torch. a) Overview spectra between 200nm and 700nm of dry and humidified air plasmas. The spectrum of the dry air plasma is dominated by NO-bands in the UV-region. When the air is moistened, OH-bands around 310nm appear in the spectrum additionally to the NO-bands. These bands can be used to determine the gas temperature of the plasma. b) Overview spectrum of a dry air plasma in the wavelength range of 200nm to 1000nm. Since the sensitivity of the spectrometer, which was used to record this spectrum, is low in the UV-range, the NO-bands are not observed. However, N_2-bands can be seen between 600nm and 1000nm. Furthermore, atomic oxygen lines at 777nm and at 844nm, which can be used to estimate the electron temperature, are observed when this spectrometer is used. c) The upper diagram shows the axial distribution of the gas temperature T_g and electron temperature T_e. The maximum value of both temperatures is reached at an axial position of 30mm with $T_e \approx 5800K$ and $T_g \approx 3000K$. Then the temperatures decrease. The lower diagram shows the radial temperatures distribution at an axial position of 30mm. It can be seen that the highest temperatures are reached in the centre. Contour plots of the gas and electron temperatures spatially resolved in axial and radial distribution are shown on the right side. Parameters: microwave power: 1kW, gas flow:10 sl/min humidified air.

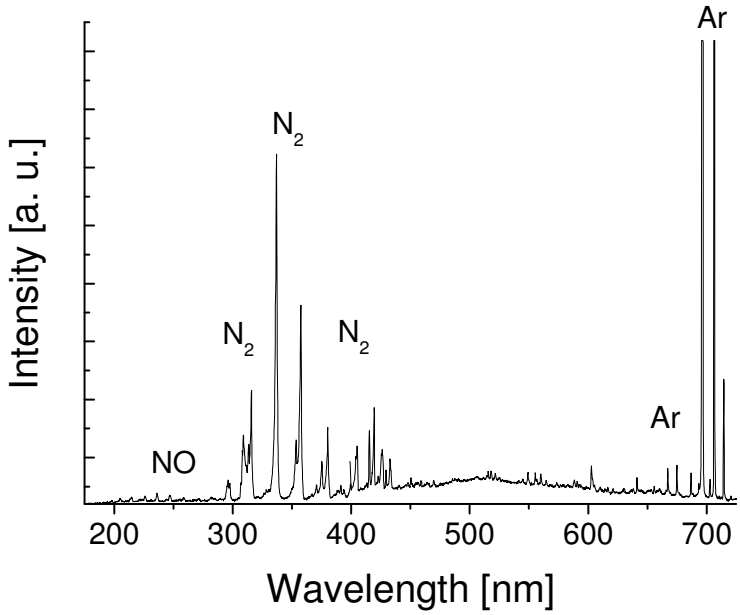

Figure 9: Overview spectrum of an argon plasma of the microwave micro plasma jet at a microwave power of about 35 W. NO-bands are observed in the UV-region between 200nm and 300nm. Between 300nm and 450nm, the spectrum shows N_2-bands, while atomic argon lines appear around 700nm.

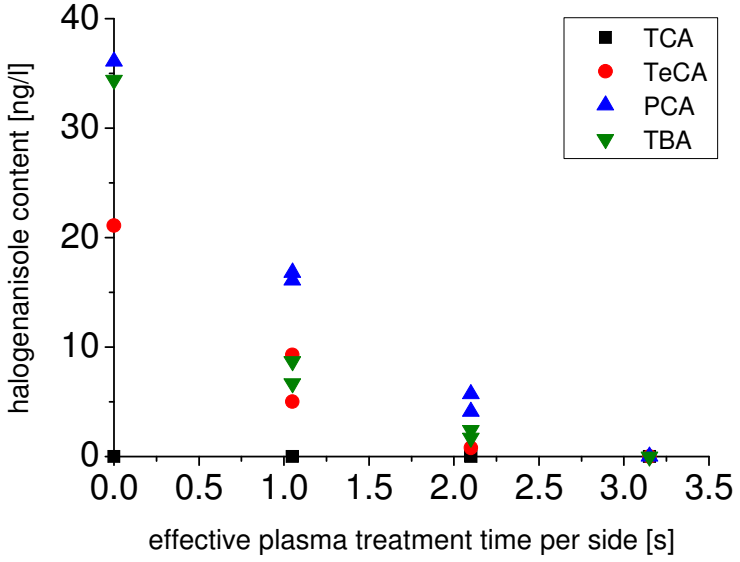

Figure 10: Results of the halogen anisole plasma decontamination experiments on PDMS foil as neutral substrate.

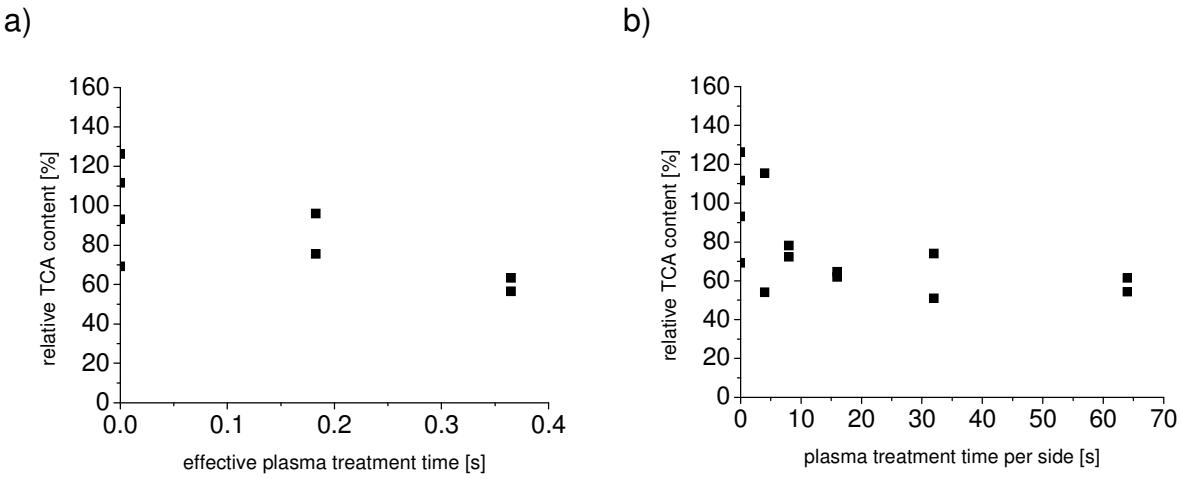

Figure 11: a) Results of halogen anisole plasma decontamination experiments on uncoated natural cork stoppers: a) microwave micro plasma jet, b) microwave plasma torch.

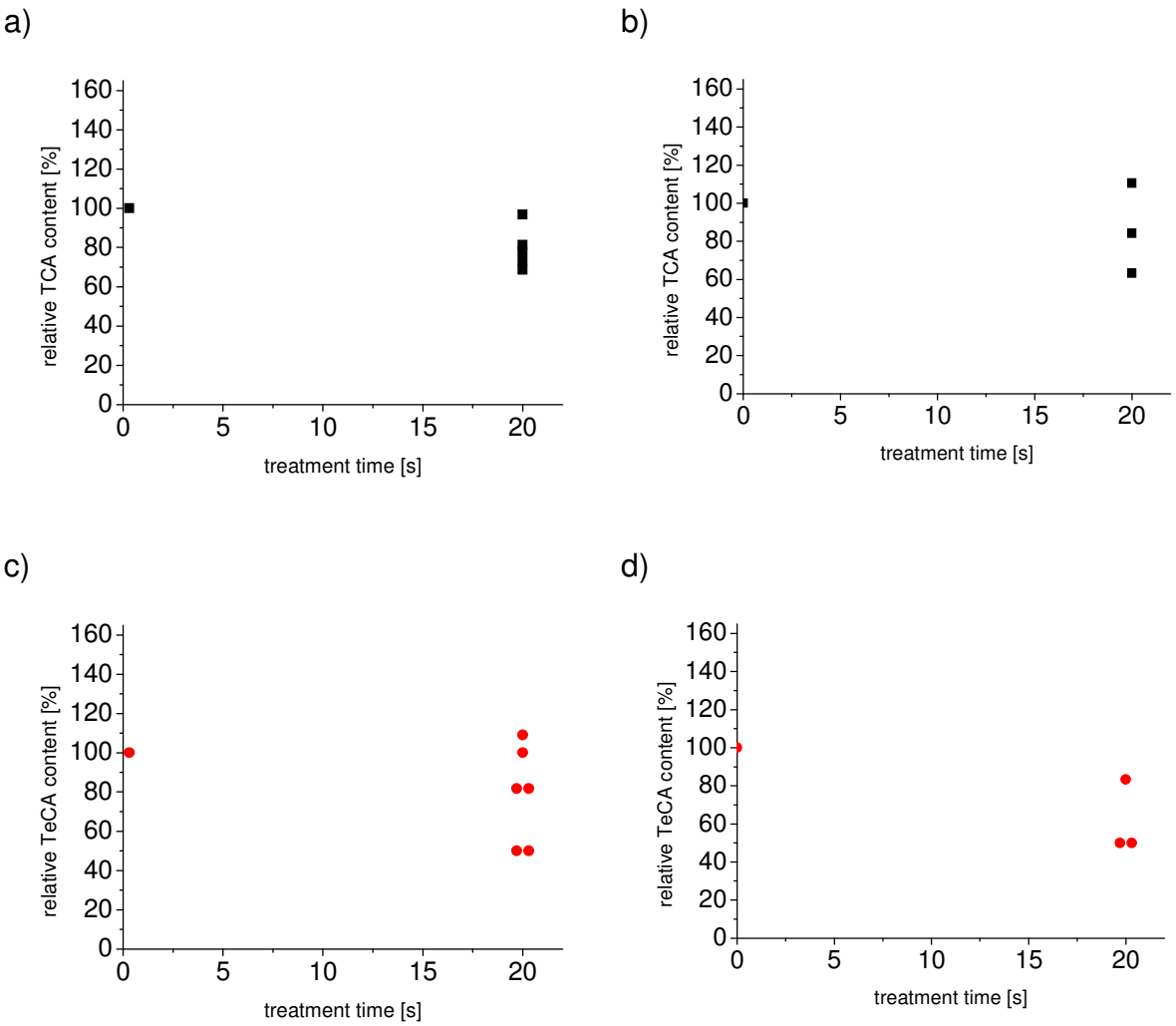

Figure 12: Results of halogen anisole plasma decontamination experiments with the corona-based plasma torch: a) TCA contamination reduction efficiencies on uncoated cork stoppers, b) TeCA contamination reduction efficiencies on uncoated cork stoppers, c) TCA contamination reduction efficiencies on with silicon and paraffin coated cork stoppers, d) TeCA contamination reduction efficiencies on with silicon and paraffin coated cork stoppers.

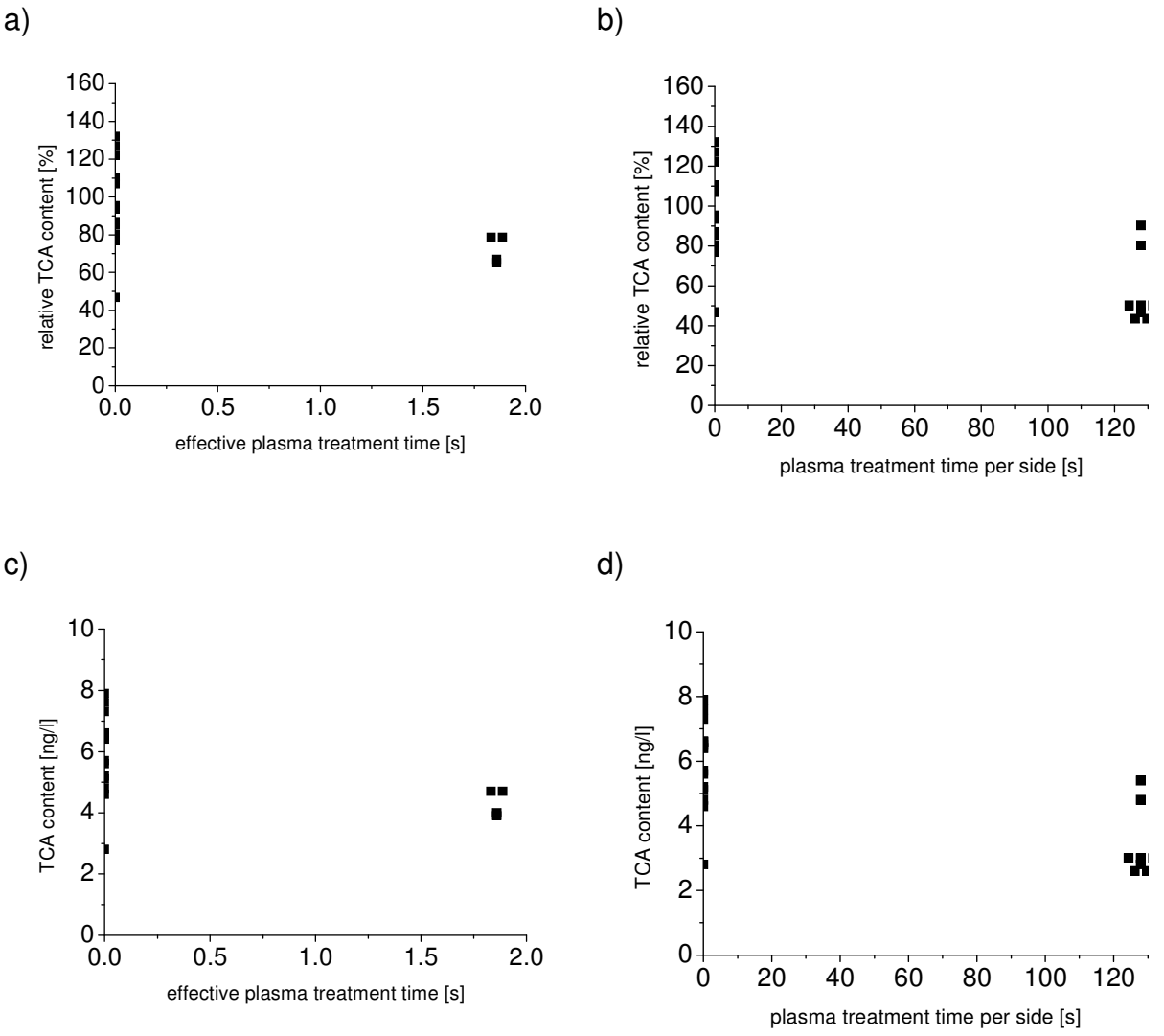

Figure 13: Results of halogen anisole plasma decontamination experiments on with silicon and paraffin coated natural cork stoppers: a) and c) microwave micro plasma jet, b) and d) microwave plasma torch.

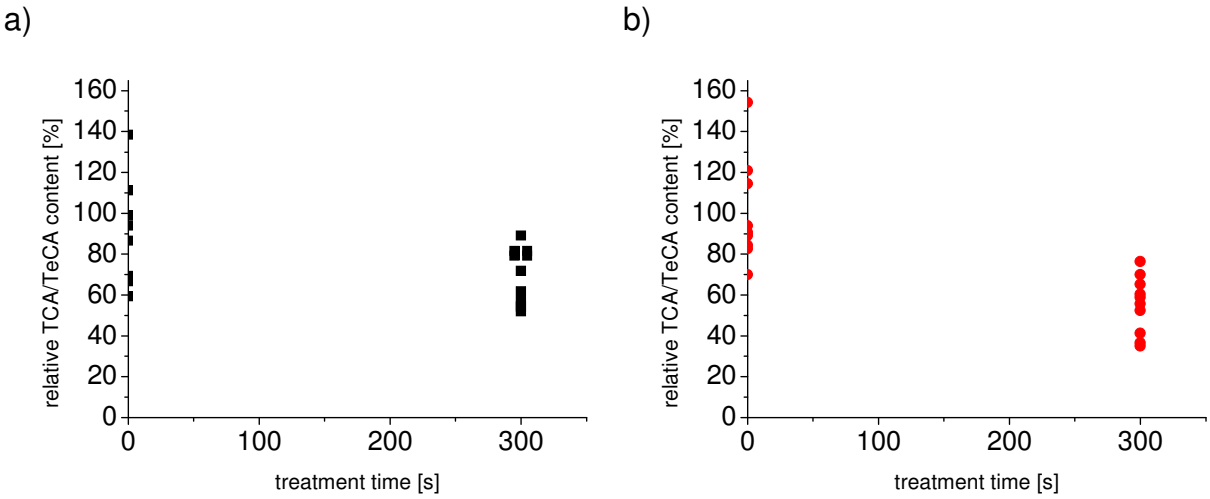

Figure 14: Results of halogen anisole plasma decontamination experiments on with silicon and paraffin coated cork disks directly exposed to the DBD plasma: a) TCA contamination reduction efficiencies, b) TeCA contamination reduction efficiencies.

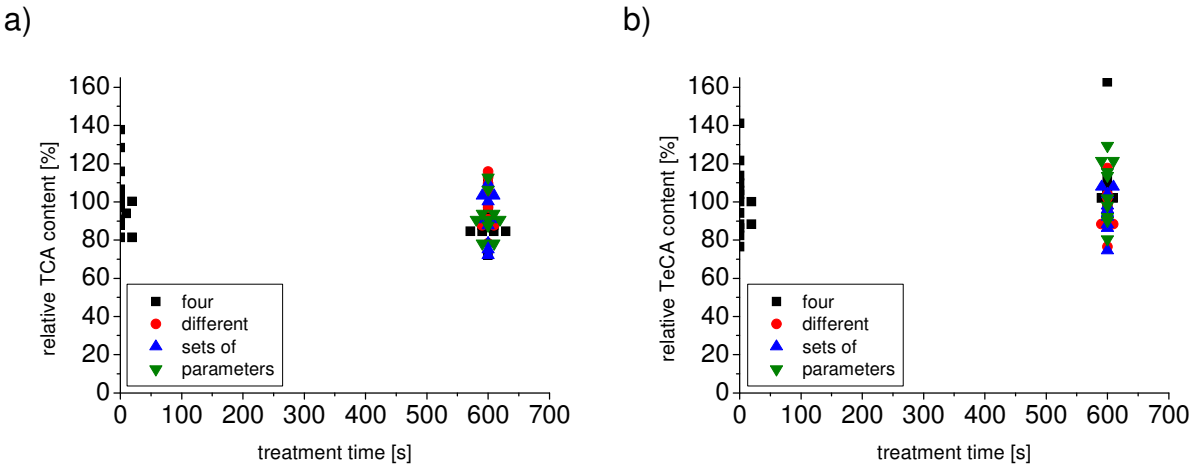

Figure 15: Results of halogen anisole plasma decontamination experiments on with silicon and paraffin coated cork stoppers by a remote DBD treatment: a) TCA contamination reduction efficiencies, b) TeCA contamination reduction efficiencies.

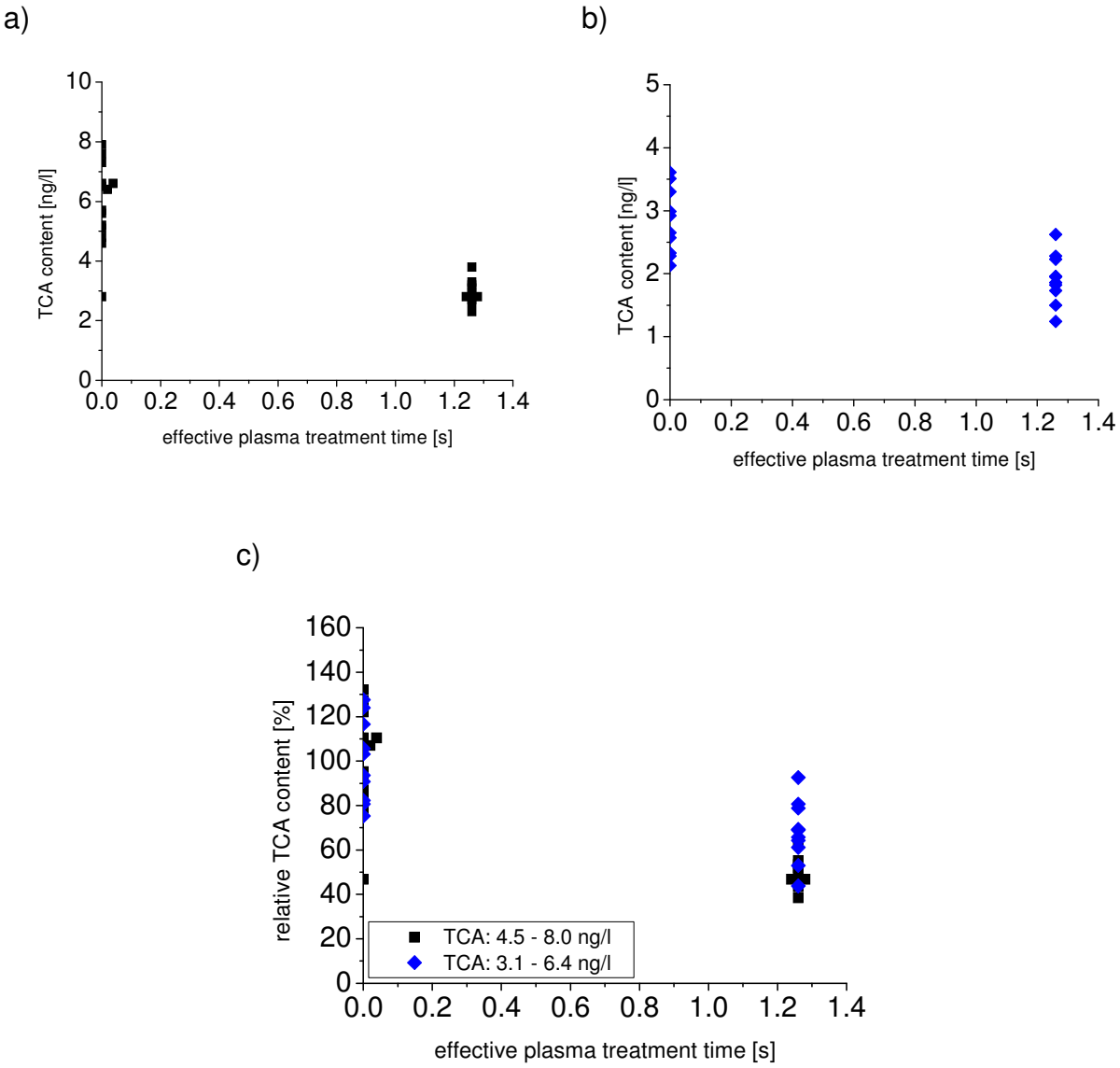

Figure 16: Results of halogen anisole plasma decontamination experiments on with silicon and paraffin coated cork stoppers with the corona-based plasma jet: a) and b) TCA contamination reduction efficiencies for two experiments with identical plasma parameters but different initial TCA contamination. c) Comparison of these two experiments.

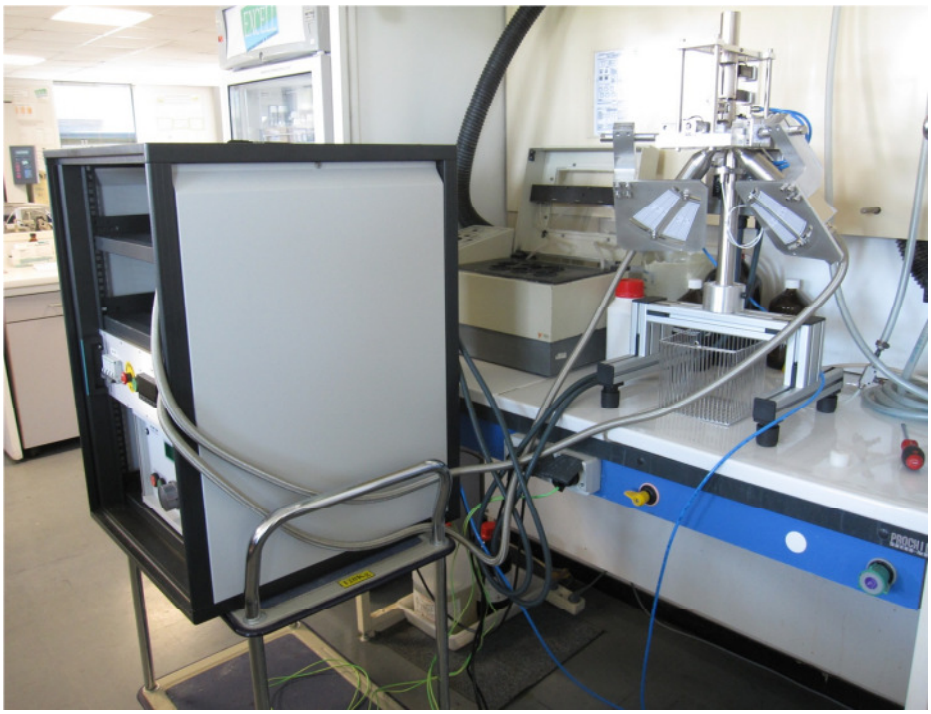

Figure 17: Photo of the NEATCORK prototype including the control unit and the mechatronics unit.

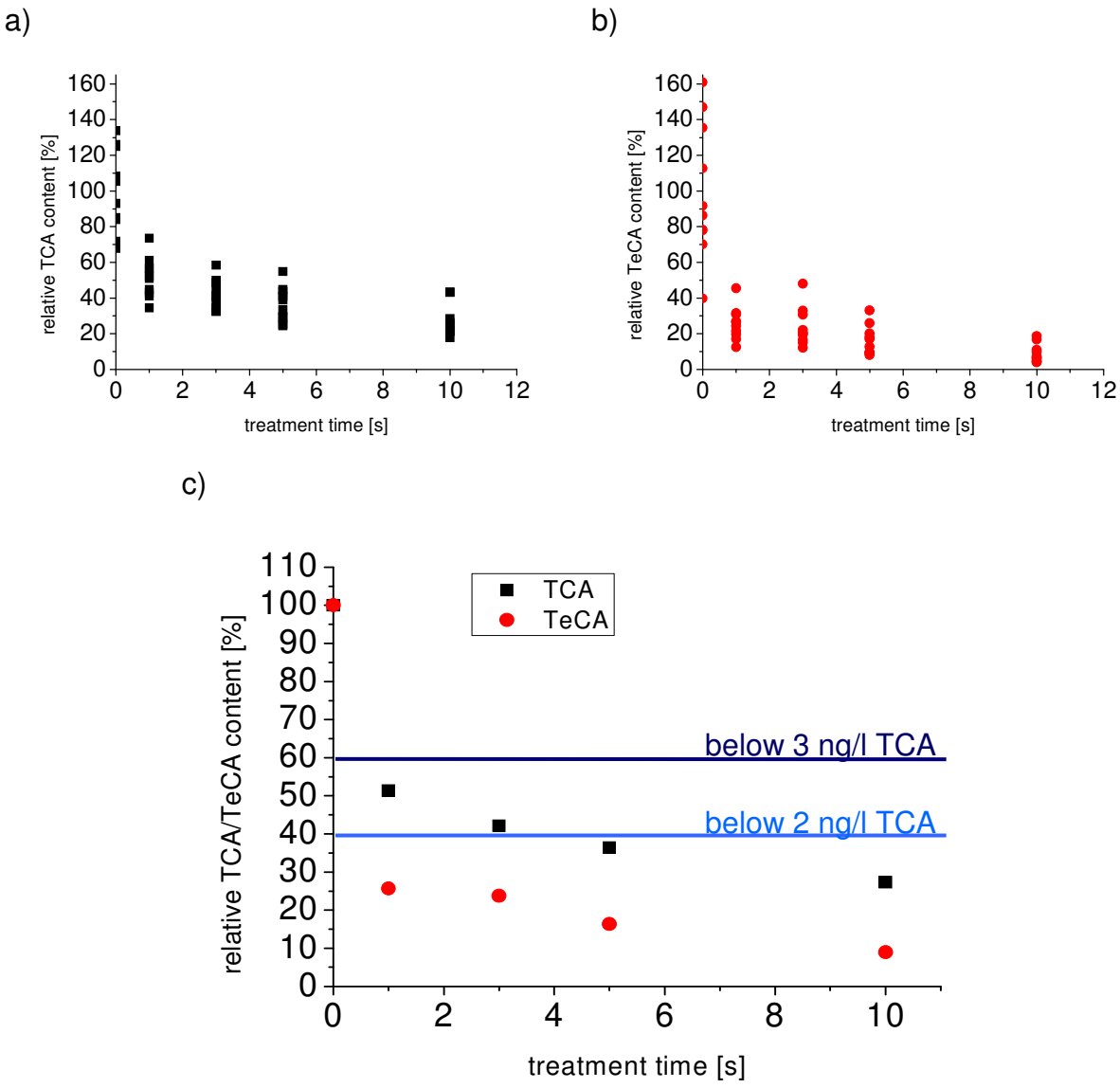

Figure 18: Results of the optimisation of the halogen anisole plasma decontamination process with the NEATCORK prototype: a) TCA contamination reduction efficiencies, b) TeCA contamination reduction efficiencies, c) an worst case initial contamination of 5ng/l TCA is assumed as 100% and the mean values of the experimental for the TCA and TeCA contamination reduction efficiencies data are plotted. Furthermore, threshold for a reduction of the TCA contamination to 3 and 2ng/l are marked.